On the sensitivity of Hybrid-Polarity features over Arctic and Antarctic regions: preliminary results

Rafael Lemos Paes[1]
Andrea Buono[2]
Ferdinando Nunziata[2]
Maurizio Migliaccio[2]

[1] Instituto Nacional de Pesquisas Espaciais (INPE), Earth Observation Coordination
12227-010, São José dos Campos - SP, Brazil
rlpaes, loren@dsr.inpe.br

[2] Dipartimento di Ingegneria, Università degli Studi di Napoli Parthenope
Centro Direzionale, isola C4, 80133 – Napoli, Italy
andrea.buono, ferdinando.nunziata, maurizio.migliaccio@uniparthenope.it

Abstract. In this study, preliminary results on the capability of Hybrid-Polarity (HP) Synthetic Aperture Radar (SAR) architectures to observe ice scenarios are presented. HP features, emulated from real fully-polarimetric L-band SAR data exploiting fundamentals of wave polarimetry concepts, are considered and tested over a large dataset consisting of 5 ALOS-PalSAR acquisitions gathered over the Svalbard Norwegian archipelago in the Arctic Ocean, and over the Terra Nova Bay in Antarctica. They represent extremely complex scenarios characterized by permanent glaciers, sea ice, snow-covered mountains, ice tongues, etc. Furthermore, the type of snow and ice covering Arctic and Antarctic lands and seas shows a strong daily and seasonal variability, making such environments very difficult to analyze. Their adverse atmospheric conditions make remote sensing a crucial tool to study such regions, which represent a key source of information about the global climate change. However, when dealing with SAR observations, the complexity of those environments in terms of scattering mechanisms makes this task not straightforward.
In this study, some meaningful experiments demonstrate the capability of HP architectures to provide valuable information on Arctic and Antarctic regions. The polarimetric set of HP features, including wave entropy, degree of polarization, complex correlation coefficient and circular polarization ratio has shown to provide interesting signatures of the different scenarios within ice areas, when combined together. However, to avoid wrong interpretations of the polarimetric results caused by terrain azimuth slopes a pre-processing step constiting of compensate the polarization angle effects due to the terrain azimuth slopes is accomplished.

Keywords: synthetic aperture radar, hybrid-polarity, ice .

1. Introduction

Ice regions represent an extremely complex scenario. They include glaciers, snow-covered mountain chains, icebergs, sea ice, ice tongues, etc. Furthermore, their characteristics as ice thickness, number of icebergs, amount of filed snow, etc. strongly vary depending on several weathering parameters as season, ocean temperature, hour of the day, moisture, wind, etc. In this sense, Arctic and Antarctic environments are very different, and such a difference in ice type and thickness, snow cover and composition, etc. has to be taken in account. The importance of ice environments mainly relies on their impact on the global climate change, but they also have a crucial role in operational activities as military operations, maritime trading, offshore drilling platforms (these regions are rich of oil, gas and mineral deposits), fishing, etc. However, such enviroments are huge and chacterized by extreme conditions adverse to

humans, thus they make remote sensing an essential tool. In this framework, the Synthetic Aperture Radar (SAR) plays a key role since it is a non-cooperative active microwave system whose imaging capabilities are independent of solar illumination and mostly unaffected by weather conditions. In literature, polarimetric SAR-based techniques aiming to study Arctic and Antarctic areas retrieving important ice parameters as ice edge, thickness, type, concentration, deformation (ridges), dynamics (drift), etc. have been proposed (KIM; KIM; HWANG, 2011; NGHIEM; BERTOIA, 2001; SCHEUCHL; HAJNSEK; CUMMING, 2002). However, Fully-Polarimetric (FP) SAR architecture comes at high costs in terms of average transmitted power, halved swath width and limited range of acceptable incidence angles with respect to a single-/dual-polarization SAR. Such drawbacks can be overcome by the Hybrid-Polarity (HP) architecture that is able to provide performance very close to the FP ones. HP SAR architecture consists of transmitting a circularly-polarized electric field while receiving coherently according to an orthogonal h-v polarization basis. Specific advantages of HP SAR architectures can be found in (SOUYRIS et al., 2007; RANEY, 2007; RANEY et al., 2011; ATTEIA; COLLINS, 2013).
In this study, HP SAR data are emulated transforming real L-band fully-polarimetric ALOS-PalSAR measurements to extract a set of polarimetric features. Experiments undertaken over a dataset composed by 5 SAR data acquired over the Arctic Svalbard archipelago and over the Antarctic Terra Nova Bay demontrated the sensitivity of such HP features to the different sea/land ice scenarios. The remainder of this paper is organized as follows: in Section 2 basic wave polarimetry concepts are presented to describe the HP SAR architecture from which the considered features are extracted; furthermore, the meaning and the basic procedure to compensate the effects of the terrain azimuth slopes are briefly shown. In Section 3 preliminary experimental results are presented and discussed, while future work is detailed in Section 4.

2. Theoretical Background

2.1. Hybrid-Polarity SAR Architecture

In real scenarios, since electric waves scattered off a distributed scene in response to an almost monochromatic illumination show partially polarized properties ranging between fully polarized and unpolarized wave ones, their description relies on second-order field correlation properties that can be obtained using the coherence matrix (BORN; WOLF, 1980),(MANDEL; WOLF, 1995),(GIL, 2007). The Hermitian and semi-positive defined 2x2 coherence matrix $\mathbf{\Gamma}$ is Hermitian can be expressed, in an orthogonal x-y basis, as (BORN; WOLF, 1980):

$$\mathbf{\Gamma} = \langle \mathbf{E}\mathbf{E}^{\dagger} \rangle = \begin{pmatrix} \langle E_x {E_x}^* \rangle & \langle E_x {E_y}^* \rangle \\ \langle E_y {E_x}^* \rangle & \langle E_y {E_y}^* \rangle \end{pmatrix} = \begin{pmatrix} \Gamma_{xx} & \Gamma_{xy} \\ \Gamma_{yx} & \Gamma_{yy} \end{pmatrix} \tag{1}$$

where, $\mathbf{E}$ is the complex electric field; † and * stand for complex conjugate transpose and complex conjugate, respectively; and a temporal dependence $e^{j\omega t}$ is considered, where ω is the angular frequency, j is the imaginary unit, and t stands for time. The correlation prevailing between the orthogonal components of the electric field is represented by the off-diagonal elements of $\mathbf{\Gamma}$. Hence, the complex correlation coefficient μ_{hv}, can be defined as (BORN; WOLF, 1980):

$$\mu_{hv} = |\mu_{hv}| e^{j\delta_{hv}} = \frac{\Gamma_{xy}}{\sqrt{\Gamma_{xx}}\sqrt{\Gamma_{yy}}} \quad ; \quad 0 \leq |\mu_{hv}| \leq 1 \, , -180^{\circ} \leq \delta_{hv} \leq +180^{\circ} \tag{2}$$

where, δ_{hv} is the phase difference between the components x and y of the received electric field. When the wave is unpolarized, μ_{hv} = 0, while a fully polarized wave presents $|\mu_{hv}|$ = 1. Basis invariant compact parameters can be used to describe the state of polarization as well

as the degree of randomness of a generic partially polarized wave. They are the degree of polarization p and the wave entropy H_w, physically representing a measure on how close the wave is fully polarized and on how far the electric field is from being completely random. They are mathematically given by (BORN; WOLF, 1980; MANDEL; WOLF, 1995; GIL, 2007):

$$p = \sqrt{1 - \frac{4det(\mathbf{\Gamma})}{tr(\mathbf{\Gamma})^2}} \quad , \; H_w = -tr(\hat{\mathbf{\Gamma}} log_2 \hat{\mathbf{\Gamma}}) \; ; \; 0 \leq p, H_w \leq 1 \tag{3}$$

where $\hat{\mathbf{\Gamma}} = \frac{\mathbf{\Gamma}}{tr(\mathbf{\Gamma})}$. p = 0 (H_w = 1) means totally unpolarized while p = 1 (H_w = 0) fully polarized wave. Additionally, in this study, the circular polarization ratio μ_c is also used which is given by (RANEY et al., 2012; SHIRVANY; CHABERT; TOURNERET, 2012):

$$\mu_c = \frac{\Gamma_{yy} + \Gamma_{xx} - 2\Im(\Gamma_{xy})}{\Gamma_{yy} + \Gamma_{xx} + 2\Im(\Gamma_{xy})} \geq 0 \tag{4}$$

where $\Im(\cdot)$ stands for imaginary part and μ_c is the ratio of the same-sense to opposite-sense circular polarization received power, performing a measure of volumetric multiple scattering. These features have been first used for ship detection in (PAES; NUNZIATA; MIGLIACCIO,) and for oil slick observation in (NUNZIATA; MIGLIACCIO; LI, 2014).

The HP architecture consists of transmitting a circularly-polarized wave while receiving coherently two orthogonal linear H and V polarizations (RANEY, 2007). In this study, a right-handed circular polarization is assumed to be transmitted. The linearly polarized received field $\mathbf{E}$ = (E_h,E_v) is emulated by the full scattering matrix $\mathbf{S}$ according to (RANEY et al., 2011; PAES; NUNZIATA; MIGLIACCIO,):

$$\mathbf{E} = \begin{pmatrix} E_h \\ E_v \end{pmatrix} = \frac{1}{\sqrt{2}} \begin{pmatrix} S_{hh} - jS_{hv} \\ S_{hv} - jS_{vv} \end{pmatrix} \tag{5}$$

where, S_{pq} with $p, q \in \{H, V\}$ is the complex scattering amplitude. Then, HP features can be emulated by wave polarimetry concepts using the following equations based on $\mathbf{\Gamma}$ (eq. (1)):

$$\begin{array}{c} \Gamma_{hh} = \frac{1}{2}(|S_{hh}|^2 + |S_{hv}|^2 + jS_{hh}{S_{hv}}^* - jS_{hv}{S_{hh}}^*) \\ \Gamma_{hv} = \frac{1}{2}(S_{hh}{S_{hv}}^* + jS_{hh}{S_{vh}}^* - j|S_{hv}|^2 + S_{hv}{S_{vv}}^*); \;\; \Gamma_{vh} = {\Gamma_{hv}}^* \\ \Gamma_{vv} = \frac{1}{2}(|S_{hv}|^2 + |S_{vv}|^2 + jS_{hv}{S_{vv}}^* - jS_{vv}{S_{hv}}^*) \; . \end{array} \tag{6}$$

2.2. Polarization Orientation angle Compensation

The polarization state of an electromagnetic wave can be geometrically described by its polarization orientation angle ψ and its ellipticity angle χ. The first, in particular, is the angle between the major axis of the generic polarization ellipse of a fully-polarized monochromatic TEM wave and the horizontal axis. When dealing with real scenarios characterized by significant azimuthal (topographical) slopes, it has to be taken in account that they induce orientation shifts causing the polarization to rotate about the line of sight. Assuming a perfect calibration of the polarimetric SAR system matched with the observed scene reference system, the presence of an azimuthal tilt on the surface patch makes its normal outside the incidence plane inducing a polarization orientation angle shift ψ. The latter rotates the incidence plane about the line of sight to the surface normal by the following (LEE; SCHULER; AINSWORTH, 2000):

$$tan\psi = \frac{tan\omega}{-tan\gamma cos\phi + sin\phi} \tag{7}$$

However, although looking eq. (7) other factors as the radar look angle ϕ and the ground range slope $tan\gamma$ can induce orientation shifts (LEE et al., 2003; POTTIER et al., 1999), the main contribute of the azimuth slope $tan\omega$ has to be compensated to provide a correct extraction and interpretation of polarimetric features. Hence, to avoid misunderstanding caused from re-polarization effects on the receveid electric field, the orientation angle has to be estimated and corrected. In literature different estimation methods have been presented, but it was demonstrated that the circular polarization method is effective, simple and accurate more than any other technique (LEE et al., 2003). In this study, the Polarization Orientation angle Compensation (POC) based on the circular polarization method is employed. Based on reflection symmetry, it consists of applying the following estimator for ψ (LEE et al., 2003):

$$\eta = \frac{1}{4}\left[tan\left(\frac{-4\Re\left(\langle(\tilde{S_{hh}} - \tilde{S_{vv}})\tilde{S_{hv}}^{*}\rangle\right)}{-\langle|\tilde{S_{hh}} - \tilde{S_{vv}}|^{2}\rangle + 4\langle|\tilde{S_{hv}}|^{2}\rangle}\right)^{-1} + \pi\right] \quad \eta \leq \pi/4 \tag{8}$$

where an extra shift of $-\pi/2$ has to be added when $\eta > \pi/4$. In eq. (8) the arctangent has to be computed in the range $(-\pi, \pi)$ and the symbol $\tilde{\mathrm{S}}$ indicates the scattering amplitude of the scattering matrix after the rotation. However, it should be noted that the whole process can be influenced by SAR parameters as the frequency, the polarimetric calibration and the dynamic range of its response. More details can be found in (LEE et al., 2003).

3. Experiments

In this section, experiments undertaken over a dataset composed by 5 L-band fully polarimetric ALOS-PalSAR data are described, and their corresponding results are shown and discussed to evaluate the sensitivity of HP features with respect to the scattering mechanisms which rule over Arctic and Antarctic regions. In particular, 3 Single-Look Complex (SLC) acquisitions (product and scene IDs: P1.1D ALPSRP177292000, P1.1A ALPSRP172381610 and P1.1A ALPSRP063271600) collected on 23 May 2009, 19 April 2009 and 2 April 2007, respectively, over the Svalbard Arctic archipelago (78.30°N, 12.30°E), and 2 SLC acquisitions (product and scene IDs: P1.1A ALPSRP177455590 and P1.1A ALPSRP177455600) gathered over the Antarctic area of the Terra Nova Bay (75.30°S, 164.60°E) are considered. After a pre-processing phase consisting of applying the POC described in Subsection 2.2 on the real fully polarimetric SAR measurements, all the HP features described in Subsection 2.1 have been computed emulating the HP SAR data from the $\mathbf{\Gamma}$ matrix of eq. (1).

In Fig. 1(a) the Google Earth image in which the observed area corresponding to the three Arctic acquisitions is shown, together with some pictures witnessing the complexity of the considered environment (see Fig. 1(b)). In fact, sea ice, glaciers, ocean and snow-covered mountains coexist all together in the Svalbard archipelago. The 18432x1088 SAR image referred to the acquisition labeled P1.1D ALPSRP177292000 (yellow rectangle in Fig. 1(a)) is shown in Fig. 1(c), where the grey-tone VV intensity channel image, in which the POC has been applyed using a 7x7 average moving window, is shown in logaritmic scale. Three different main scenarios can be identified in Fig. 1(b): some homogeneous low-basckattering areas on the left side, some homogeneous regions with larger backscattering especially in the middle of the SAR image, and several areas characterized by a typical relief backscattering pattern spreaded over the whole image. Hence, the sensitivity of each polarimetric HP feature, computed using a 3x3 average sliding window, with respect to such a variegated environment, is investigated. In Fig. 2 experimental results related to the SAR image of Fig. 1(b) are shown. From a first visual inspection, all the considered HP features are able to provide scattering

information on the different scenarios, exhibiting different responses varying the scattering mechanism which rules over each region. In detail, $|\mu_{hv}|$, δ_{hv}, μ_c, H_w and p images are shown in Fig. 2(a)-(e), respectively. Since the other two L-band fully polarimetric ALOS-PalSAR data considered in this study provided similar results, they are not shown for the sake of brevity. In Fig. 3(a) the Google Earth image referred to the two Antarctic acquisitions considered in this study are shown, which are placed over thr Ross Sea and where the Drygalski ice tongue is clearly visible. Furthermore, some meaningful Google Earth images, witnessing the environmental complexity of the Antarctic scenario and its significant differences with respect to the Arctic one showed in Fig. 1(a), are shown in Fig. 3(b). The 18432x1088 HH intensity gray-tone image (product and scene ID: P1.1A ALPSRP177455590), in which the POC has been applyed using a 7x7 average moving window, is shown in Fig. 3(c) in logaritmic scale. Three different main scenarios can be identified in Fig. 3(b): some homogeneous low-basckattering areas on the left side, some homogeneous regions with larger backscattering especially in the middle of the SAR image, and several areas characterized by a typical relief backscattering pattern spreaded over the whole image. Hence, the sensitivity of each polarimetric HP feature, computed using a 7x7 average sliding window, with respect to such a variegated environment, is investigated. In Fig. 4 experimental results related to the SAR image of Fig. 3(b) are shown.Highest backscattering values, here, regard to the ice tongue which one is very well differentiated from the sea by δ_{hv}, $|\mu_{hv}|$, and p. Sea ice can be also noted through all HP features because the sea responds as expected, despite it is predominantly agitated in that region, i.e., δ_{hv} is about 90° and $|\mu_{hv}|$ is high. Another observable characteristic is that sea ice presents a backscattering lower than the sea for L-band (ONSTOTT, 2004), but presents polarimetric characteristics similiar to the ice tongue.

4. Future Work

In this study, the sensitivy of HP features, computed emulating actual fully-polarimetric L-band ALOS-PalSAR data, is investigated with respect to their capability to monitor ice regions. Although the lack of ground truthed information makes the interpretation of polarimetric results very difficult, preliminary results seem very interesting. In particular, combining the polarimetric scattering information carryed on by the considered HP features set, composed by μ_{hv}, μ_c, H_w and p, interesting details regarding the scattering mechanisms which characterized the observed scene can be inferred. The environmental importance of such scenarios makes deeper studies strongly needed. Hence, future works can be involved proper in situ measurement campaigns to collect the crucial ground truth information about ice thickness, snow composition, etc. and also the development of ad hoc calibration procedures to extract scattrign information from polarimetric SAR observations in the most correct way.

Referências

ATTEIA, G. E.; COLLINS, M. J. On the use of compact polarimetry sar for ship detection. *ISPRS Journal of Photogrammetry and Remote Sensing*, v. 80, p. 1–9, 2013.

BORN, M.; WOLF, E. *Principles of optics*. [S.l.]: Cambridge University Press, London, 1980.

GIL, J. J. Polarimetric characterization of light and media. *The European Physical Journal Applied Physics*, v. 40, n. 1, p. 1–47, 2007.

KIM, J. W.; KIM, D. J.; HWANG, B. J. Characterization of arctic sea ice thickness using space-borne polarimetric sar data. In: IGARSS, 2011, Vancouver, BC, Canada. *IGARSS*. [S.l.]: IEEE International, 2011. p. 2105–2108.

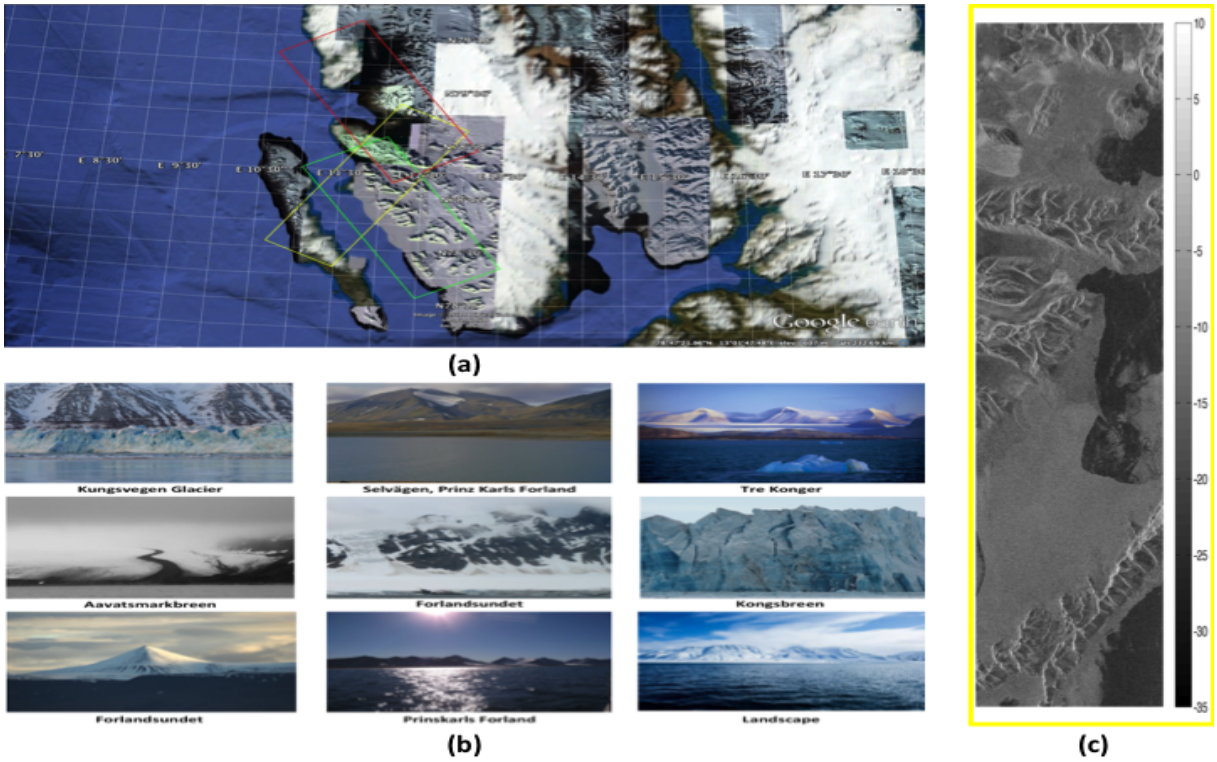

Figura 1: (a) Google Earth image in which the three L-band fully-polarimetric ALOS-PalSAR acquisitions over the Arctic Svalbard area considered in this study. (b) Example images of the complex Arctic environment in the Svalbard archipelago, in which very different kinds of scenario can be encountered: glaciers, sea ice, mountains, ocean, snow covered reliefs, etc. (source Google Earth). (c) Grey-tone VV intensity image, in logaritmic scale, relevant to the acquisition P1.1D ALPSRP177292000 gathered over the Svalbard Norwegian archipelago (yellow rectangle in Fig. 1(a)), in which the POC is applyed using a 7x7 average sliding window.

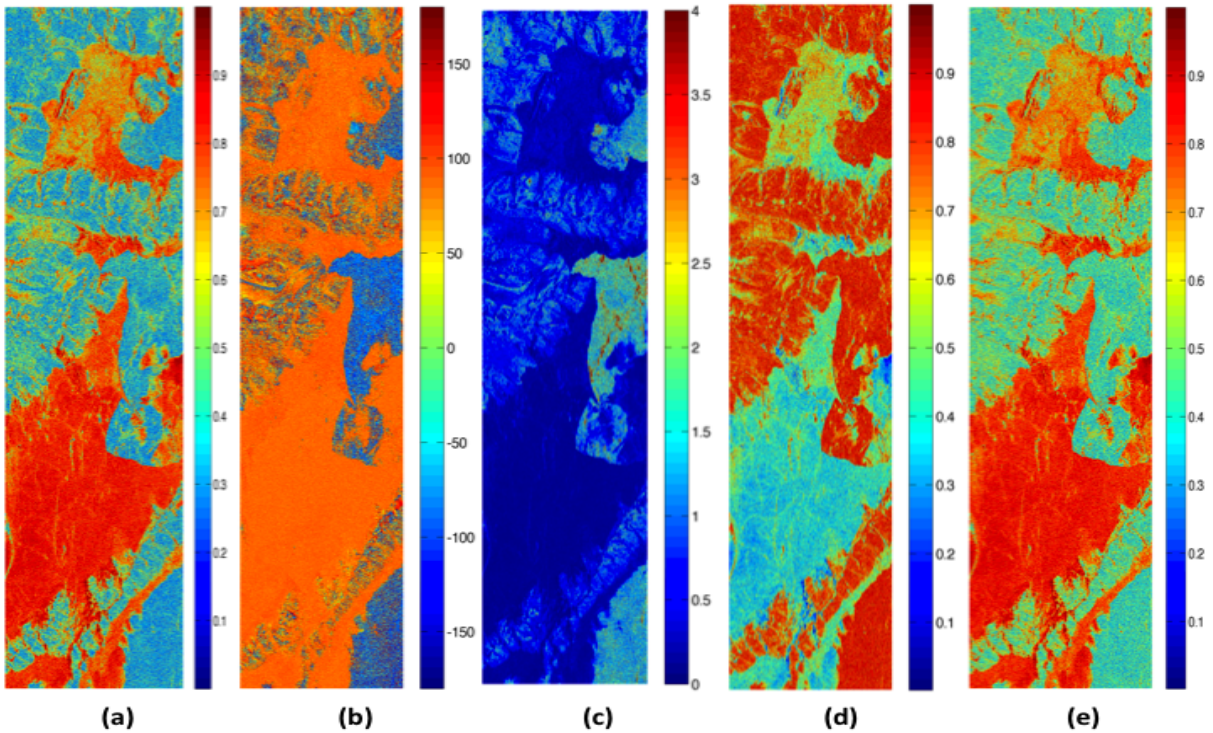

Figura 2: HP features results related to the acquisition shown in Fig. 1(b) and computed using a 3x3 average moving window: (a) $|\mu_{hv}|$ image, (b) δ_{hv} image, (c) μ_c image, (d) H_w image, (e) p image.

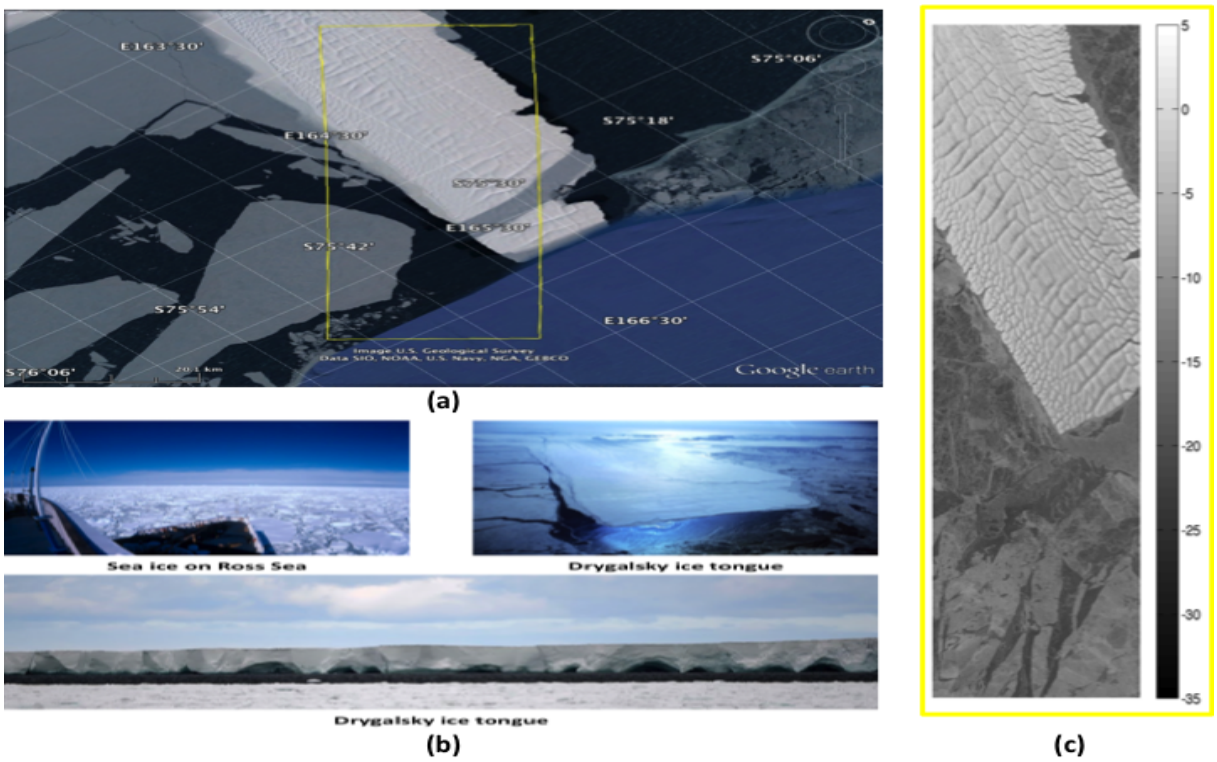

Figura 3: (a) Google Earth image in which the three L-band fully-polarimetric ALOS-PalSAR acquisitions over the Antarctic Terra Nova Bay area considered in this study. (b) Pictures of typical ice formation presents in the complex Antarctic environment in the Terra Nova Bay: sea ice over the Ross Sea and the Drygalski ice tongue (source Google Earth). (c) Grey-tone HH intensity image, in logaritmic scale, relevant to the acquisition P1.1A ALPSRP177455590 gathered over the Terra Nova Bay (yellow rectangle in Fig. 3(a)), in which the POC is applyed using a 7x7 average moving window.

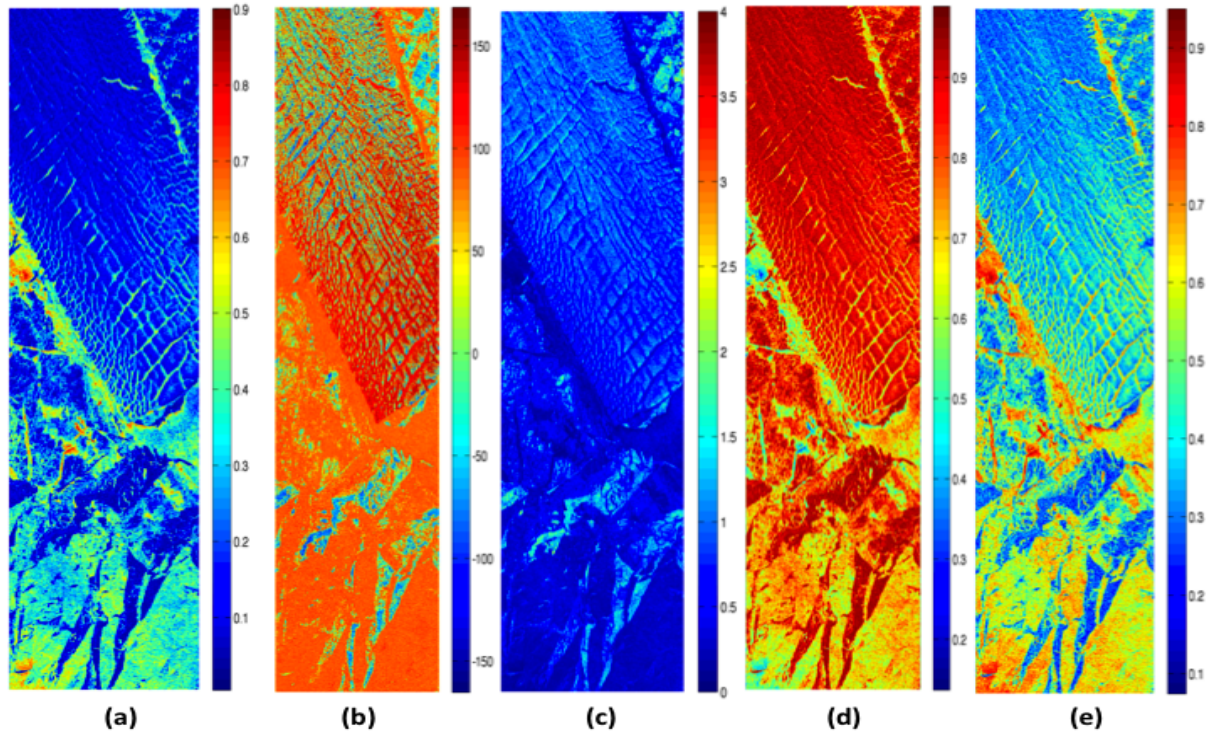

Figura 4: HP features results, relevant to the acquisition shown in Fig. 3(b), evaluated using a 7x7 average moving window: (a) $|\mu_{hv}|$ image, (b) δ_{hv} image, (c) μ_c image, (d) H_w image, (e) p image.

LEE, J. S.; SCHULER, D. L.; AINSWORTH, T. I. Polarimetric sar data compensation for terrain azimuth slope variation. *IEEE Trans. Geosci. Remote Sens.*, v. 38, n. 5, p. 2153–2163, 2000.

LEE, J. S. et al. Polarization orientation estimation and applications: a review. In: PROCEEDINGS OF THE IEEE, 2003. *Geosci. Remote Sens. Symp. IGARSS*. [S.l.]: IEEE International, 2003. v. 1, p. 428–430.

MANDEL, L.; WOLF, E. *Optical coherence and quantum optics*. [S.l.]: Cambridge University Press, NY, 1995.

NGHIEM, S. V.; BERTOIA, C. Study of multi-polarization c-band backscatter signatures for arctic sea ice mapping with future satellite sar. *Can. J. Remote Sens.*, v. 27, n. 5, 2001.

NUNZIATA, F.; MIGLIACCIO, M.; LI, X. Sea oil slick observation using hybrid-polarity sar architecture. *J. Ocean. Engin.*, PP, n. 99, p. 1–15, 2014.

ONSTOTT, R. G. Noaa sar manual. In: ____. [S.l.]: NOAA, Washington DC, 2004. cap. 19 Antarctic Sea Ice and Icebergs, p. 397–415.

PAES, R. L.; NUNZIATA, F.; MIGLIACCIO, M. On the capability of hybrid-polarity features to observe metallic targets at sea. Submitted on J. Ocean. Engin., 2014.

POTTIER, E. et al. Estimation of the terrain surface azimuthal/range slopes using polarimetric decomposition of polsar data. In: PROCEEDINGS OF IGARSS, 1999. *Geosci. Remote Sens. Symp. IGARSS*. [S.l.], 1999. v. 1, p. 2212–2214.

RANEY, R. K. Hybrid-polarity sar architecture. *IEEE Trans. Geosci. Remote Sens.*, v. 45, n. 11, p. 3397–3404, 2007.

RANEY, R. K. et al. The m-chi decomposition of hybrid dual-polarimetric radar data with application to lunar craters. *J. Geophys. Res.*, v. 117, n. 21, 2012.

RANEY, R. K. et al. The lunar mini-rf radars: hybrid polarimetric architecture and initial results. In: *Proceedings of IEEE*. [S.l.: s.n.], 2011. v. 99, n. 5, p. 808–823.

SCHEUCHL, B.; HAJNSEK, I.; CUMMING, I. Sea ice classification using multi-frequency polarimetric sar data. In: IGARSS, 2002, Toronto, Ontario, Canada. *IGARSS*. [S.l.], 2002.

SHIRVANY, R.; CHABERT, M.; TOURNERET, J. Ship and oil-spill detection using the degree of polarization in linear and hybrid/compact dual-pol sar. *J. Sel. Topics Appl. Earth Observ.*, v. 5, n. 3, p. 885–892, 2012.

SOUYRIS, J. C. et al. Sar compact polarimetry (cp) for earth observation and planetology: concept and challenges. In: POLINSAR. Frascati: ESA-ESRIN, 2007.